arXiv:1304.4728v1 [cond-mat.str-el] 17 Apr 2013

Magnetic structure of the frustrated $S = 1/2$ chain magnet $LiCu_2O_2$ doped with nonmagnetic Zn

A.A. Bush,[1] N. Büttgen,[2] A.A. Gippius,[2, 3] V.N. Glazkov,[4, 5] W. Kraetschmer,[2] L.A. Prozorova,[4] L.E. Svistov,[4, *] A.M. Vasiliev,[4] A. Zheludev,[5] and A.M. Farutin[4, 6]

[1] *Moscow State Technical University of Radioengineering,*
Electronics and Automation, 119454, Moscow, Russia
[2] *Center for Electronic Correlations and Magnetism EKM,*
Experimentalphysik V, Universität Augsburg, D–86135 Augsburg, Germany
[3] *Moscow State University, 119899, Moscow, Russia*
[4] *P. L. Kapitza Institute for Physical Problems RAS, 119334 Moscow, Russia*
[5] *Neutron Scattering and Magnetism, Laboratory for Solid State Physics,*
ETH Zürich, Switzerland, 8093 Zürich, Switzerland
[6] *Laboratoire Interdisciplinaire de Physique, CNRS et Université*
J.Fourier-Grenoble I, BP 87, 38402 Saint-Martin d'Herès, France

(Dated: April 18, 2013)

We present the results of magnetization, ESR and NMR measurements on single crystal samples of the frustrated $S = 1/2$ chain cuprate $LiCu_2O_2$ doped with nonmagnetic Zn^{2+}. As shown by the x-ray techniques the crystals of $Li(Cu_{1-x}Zn_x)_2O_2$ with $x < 0.12$ are single-phase, whereas for higher Zn concentrations the samples were polyphase. ESR spectra for all monophase samples ($0 \leq x < 0.12$) can be explained within the model of a planar spin structure with a uniaxial type anisotropy. The NMR spectra of the highly doped single crystal sample $Li(Cu_{0.9}Zn_{0.1})_2O_2$ can be described in the frame of a planar spin glass like magnetic structure with short range spiral correlations in the crystal (ab)-planes with strongest exchange bonds. The value of magnetic moments of Cu^{2+} ions in this structure is close to value obtained for undoped crystals: $(0.8 \pm 0.1)\ \mu_B$.

PACS numbers: 75.50.Ee, 76.60.-k, 75.10.Jm, 75.10.Pq

I. INTRODUCTION

$LiCu_2O_2$ is an example of $S = 1/2$ magnet with frustrated exchange interactions. The magnetic structure of $LiCu_2O_2$ can be considered as a system of coupled $S = 1/2$ chains of magnetic Cu^{2+} ions. Within the chains the nearest spins interact ferromagnetically and the next-nearest neighbors antiferromagnetically. Interest in magnetic systems with such a type of frustration is stimulated by theoretical predictions of unusual magnetic phases for uncoupled and weakly coupled (1D and quasi-1D) chain models (see for example Refs. 1,2). It was shown that a new type of magnetic ordering can be realized for the magnets with this particular type of frustration. Such a type of magnetic order, with zero average magnetic moment on each magnetic ion, but with long-range ordered correlations of spin components of neighboring ions, is classified as spin-nematic order.[3] The possibility to find this new type of magnetic order experimentally is a very attractive task. According to Ref.1, for the 1D model with the intrachain exchange constants of $LiCu_2O_2$ a chiral long-range order in the low-field range and a quasi long-range ordered spin-density wave phase in higher applied magnetic fields H are expected. In the experiment the planar spiral spin structure was observed at $T < T_N$ in the low-field range in $LiCu_2O_2$.[4,5] At higher fields $\mu_0 H \approx 15$ T another magnetic phase, which is not identified yet, was observed.[6] Probably, this phase is related to a spin-density wave phase which is predicted for the 1D model. A spin-nematic phase for the exchange integrals of $LiCu_2O_2$ is expected in even higher magnetic fields which are hardly accessible experimentally. The investigation of the zinc-doped crystals of $LiCu_2O_2$ was reported recently[7] and new magnetic phases in this system were announced. This report has stimulated the Electron Spin Resonance (ESR) and Nuclear Magnetic Resonance (NMR) investigations of the magnetic structure of Zn-doped $LiCu_2O_2$ single crystals reported here.

In the first section a short overview of the literature data about the crystal and magnetic structures of the undoped samples of $LiCu_2O_2$ is given. In the second section of the paper the details of crystal growth and sample characterization are described. In the next two sections results of ESR and NMR experiments are presented. These experiments have shown that the main features of the low-frequency dynamics of the doped samples in the magnetically ordered phase are the same as for the undoped samples. ESR spectra for the undoped and doped samples can be well described using a model of a planar spin structure with strong easy-plane anisotropy for the vector **n** normal to the spin plane.

The NMR study of the $Li(Cu_{1-x}Zn_x)_2O_2$ single crystal with $x = 0.1$ at $T < T_N$ shows the coexistence of static correlations of magnetic moments corresponding to the magnetic structure of the undoped material and, simultaneously, a static random distribution of spin directions. The temperature evolution of NMR spectra can be described by an increase of short range correlations along the crystallographic **c**-direction with decrease of the temperature. For the temperatures up to $T_N/2$ the NMR spectra can be described in the model of uncorrelated (ab) spin planes.

II. CRYSTALLOGRAPHIC AND MAGNETIC STRUCTURES OF LICU$_2$O$_2$

LiCu$_2$O$_2$ crystallizes in an orthorhombic system (space group $Pnma$) with unit cell parameters $a = 5.73$ Å, $b = 2.86$ Å and $c = 12.42$ Å.[8] The unit cell parameter a is approximately twice the unit cell parameter b. Consequently, the LiCu$_2$O$_2$ samples, as a rule, are characterized by twinning due to the formation of crystallographic domains rotated by 90° around their common crystallographic c-axis.

The unit cell of the LiCu$_2$O$_2$ crystal contains four univalent nonmagnetic Cu$^+$ cations and four divalent Cu^{2+} cations with spin $S = 1/2$. There are four crystallographic positions of the magnetic Cu^{2+} ions in the crystal unit cell of LiCu$_2$O$_2$, conventionally denoted as α, β, γ and δ.

The Cu^{2+} ions in the different positions are weakly magnetically coupled and form four almost independent systems of spin chains. Such chains formed by one of four kinds of Cu^{2+} ions (e.g. the α-position) and relevant exchange interactions[9] within the system are shown schematically in Fig. 1a.

The positions of Cu^{2+} and Li$^+$ ions in the crystal cell are given by copper coordinates[8]: (0.876; 0.75; 0.095), (0.376; 0.75; 0.405), (0.624; 0.25; 0.595), (0.124; 0.25; 0.905) and by lithium coordinates: (0.376;0.75;0.068), (0.876;0.75;0.432),(0.124;0.25;0.568),(0.624;0.25;0.932). Schematic arrangement of the Cu^{2+} and Li$^+$ ions in the projection of the crystal lattice onto the ac-plane is given in Fig. 1b

The transition into the magnetically ordered state occurs via two stages at $T_{c1} = 24.6$ K and $T_{c2} = 23.2$ K.[10] Neutron scattering and NMR experiments have revealed that an incommensurate magnetic structure is realized in the magnetically ordered state ($T < T_{c1}$).[4,5,11] The wave vector of the incommensurate magnetic structure coincides with the chain direction (the **b**-axis). The magnitude of the propagation vector at $T < 17$ K is almost temperature independent and is equal to $0.827\times 2\pi/b$. The neutron scattering experiments have shown that the neighboring magnetic moments along the **a**-direction are antiparallel, whereas those along the **c**-direction are parallel. The investigation of the spin-wave spectra by inelastic neutron scattering[9] shows that the incommensurate magnetic structure in LiCu$_2$O$_2$ is caused by a competition between the ferromagnetic exchange interaction of the nearest-neighbor magnetic ions in the chain $J_1 = -7.00$ meV and the antiferromagnetic interaction of the next-nearest neighbor ions in the chain $J_2 = 3.75$ meV. The antiparallel orientation of the magnetic moments of Cu^{2+} between neighboring chains is caused by the strong antiferromagnetic interaction $J_3 = 3.4$ meV. The coupling of the Cu^{2+} magnetic moments along the **c**-direction and the couplings between the magnetic ions in different crystallographic positions α, β, γ or δ are much weaker.[5,9] Thus, the magnetic structure of LiCu$_2$O$_2$ in the magnetically ordered phase can be considered as quasi-two dimensional. The quasi-two-dimensional character of the magnetic interactions in LiCu$_2$O$_2$ was also proven by resonant soft X-ray magnetic scattering experiments.[12,13]

The magnetic structure of LiCu$_2$O$_2$ at zero magnetic field was studied using different experimental methods, but so far there is no generally accepted model for it. For a review of proposed models see, for example, Ref. 6.

In magnetic fields above 3 T, the magnetic structure realized in LiCu$_2$O$_2$ is much clearer. ESR and NMR studies of LiCu$_2$O$_2$ in the low-temperature magnetically ordered phase ($T < T_{c2}$) established that a planar spiral magnetic structure is formed in this compound.[14] The magnetic moments located at the α (β, γ or δ) position of the crystal unit cell with coordinates x, y, z (measured along the **a**, **b** and **c**-axis of the crystal, respectively) are defined as:

$$\begin{aligned}\boldsymbol{\mu}_\alpha = \mu\cdot\mathbf{l}_1(-1)^{x/a}\cdot\cos(k_{ic}\cdot y+\phi_\alpha)+\\ +\mu\cdot\mathbf{l}_2(-1)^{x/a}\cdot\sin(k_{ic}\cdot y+\phi_\alpha),\end{aligned} \tag{1}$$

where $\mathbf{l}_1$ and $\mathbf{l}_2$ are the two mutually perpendicular unit vectors, $\mathbf{k}_{ic}$ is the incommensurability vector parallel to the chain direction (**b**-axis), μ is the magnetic moment of the Cu^{2+} ion and x is a multiple of the chain period a. The magetic moment per copper ion at $T \lesssim 10$ K was evaluated as $\mu = 0.85\ \mu_B$.[4,14] The phases ϕ_α, ϕ_β, ϕ_γ and ϕ_δ determine the mutual orientation of the spins in the chains formed by the ions in the different crystallographic positions. Their values are extracted from the NMR data[14,15]: $\phi_\alpha = 0$; $\phi_\beta = \phi_\alpha + \pi/2$; $\phi_\gamma = \pi - k_{ic} * b/2$; $\phi_\delta = \phi_\gamma + \pi/2$.

III. SAMPLE PREPARATION AND EXPERIMENTAL DETAILS

Single crystals of Li(Cu$_{1-x}$Zn$_x$)$_2$O$_2$ with the size of several cubic millimeters were prepared by the "solution in the melt" method.[16] Samples were grown in air by a flux method in alundum crucibles. The mixtures of analytical grade Li$_2$CO$_3$, CuO and ZnO of Li$_2$CO$_3$·4(1-x)CuO·4xZnO compositions were melted at 1100 °C, and then solidified by cooling to 930 °C at a rate of 5.0 °C/hour. Next, the crucible was withdrawn from the furnace and placed on a massive copper plate to ensure rapid cooling to room temperature. Quenching from ≈900 °C was necessary, because the single phase LiCu$_2$O$_2$ single crystals decompose below this temperature.[16]

The samples were shaped as a flat plates with the developed (ab)-plane. The twinning structure of the samples was studied with optical polarization microscopy.[6] In

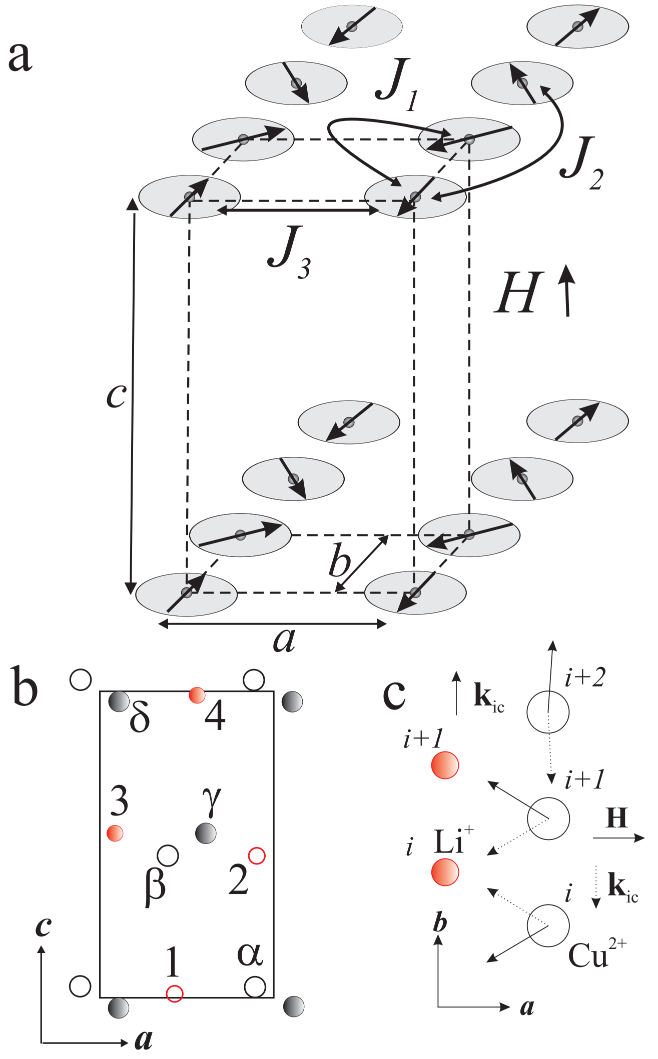

FIG. 1: a. (color online) Schematic representation of the arrangement of Cu^{2+} moments in $LiCu_2O_2$. Only one of four Cu^{2+} (α, β, γ, δ) positions is shown. Arrows correspond to the spin directions below T_{c2} for $\mathbf{H} \parallel \mathbf{c}$. J_1, J_2 and J_3 are the main exchange integrals.[9] b. Schematic arrangement of the Cu^{2+} and Li^+ ions in the projection of the crystal lattice onto the ac-plane[14]. Large circles indicate the Cu^{2+} ions, and small circles – the Li^+ ions. Closed and open circles represent ions with the coordinates equal to $0.25b$ and $0.75b$ along the b-axis, respectively. c. Scetch of the spin configuration corresponding to the extreme values of dipolar field on Li site for two incommensurable domains with incommensurability vector directed upchain (solid arrows) or downchain (dashed arrows). All spins vectors and external field are in plane of figure.

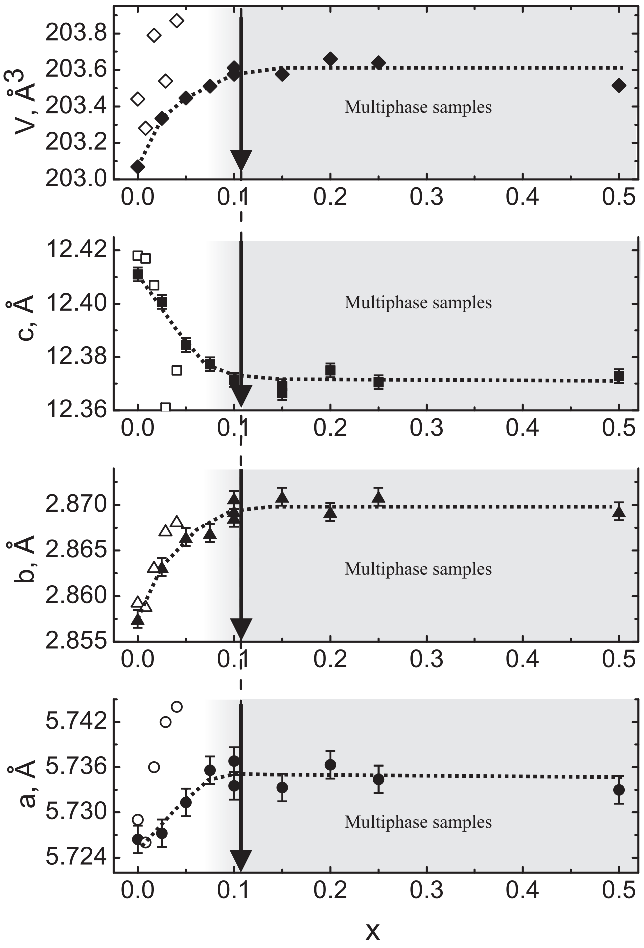

FIG. 2: The concentration dependence of the crystal unit cell volume (top panel) and crystal unit cell parameters a,b,c (lower panels) of single crystals of $Li(Cu_{1-x}Zn_x)_2O_2$. x − concentration of zinc in initial charge. The solid symbols show the results obtained on our samples discussed here. The open symbols show the data taken from Ref. 7.

most cases, the samples were twinned with a characteristic domain size of several microns. It was possible to select samples without twinning structure for Zn concentrations up to $x = 0.1$. The absence of the twinning structure in the samples selected for the experiments was confirmed by X-ray diffraction and ESR measurements.[6,14] We have used samples without twinning for most of the experiments described below.

The X-ray diffraction patterns were taken in a $\theta - 2\theta$ geometry using CuKα irradiation. The samples produced clearly distinguishable diffraction patterns from the (bc)- and the (ac)-planes of the crystal. The spectra obtained from twinned samples had a form of a superposition of these spectra. The Zn doping of $LiCu_2O_2$ results in a monotonic change of the cell parameters up to a concentration limit of $x_c \approx 0.12$. For samples with zinc content of initial charge $x < 0.12$ no diffraction patterns due to impurity phases were observed. Additional x-ray diffraction patterns were observed for the samples with $x \geq 0.12$, which can be ascribed to the presence of inclusions of impurity phases. The patterns ascribed to the main phase show that the cell parameters for higher Zn content do not change. The zinc concentrations of $Li(Cu_{1-x}Zn_x)_2O_2$ single crystals were measured by electron probe micro analysis on the spectrometer “Eagle II” (“EDAX”, USA). The concentration values of x in

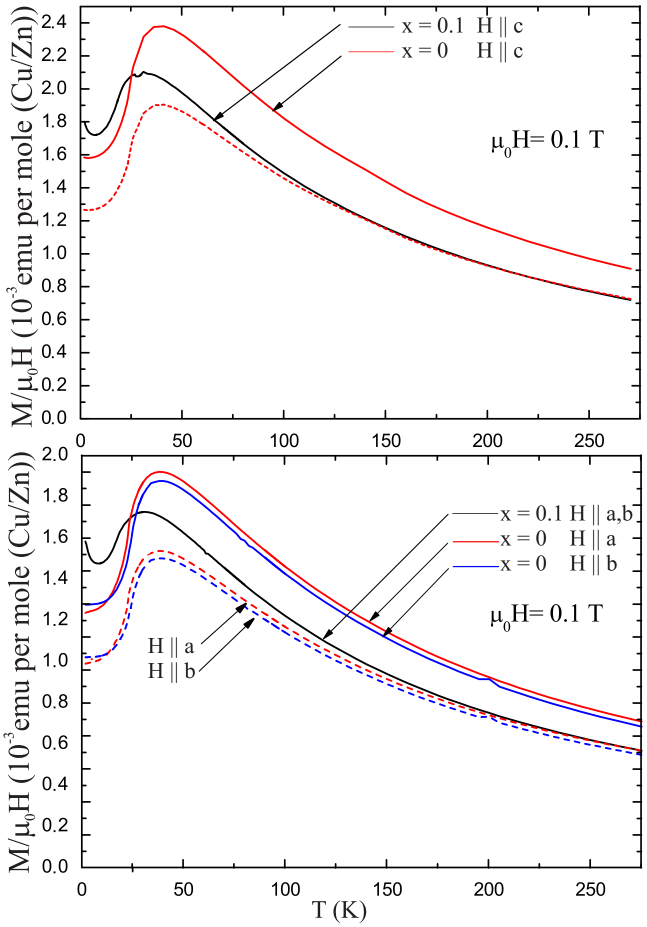

FIG. 3: (color online) Temperature dependencies of the magnetic susceptibility $M(T)/\mu_0 H$ for field directions $\mathbf{H} \parallel \mathbf{a}, \mathbf{b}$ (lower panel) and $\mathbf{c}$ (upper panel) and $\mu_0 H = 0.1$ T for a twinned doped single crystal of $\mathrm{Li(Cu}_{1-x}\mathrm{Zn}_x)_2\mathrm{O}_2$ with $x = 0.1$ (black lines) and for the undoped untwinned crystal $x = 0$ at $\mathbf{H} \parallel \mathbf{a}, \mathbf{b}$ and $\mathbf{c}$ taken from Ref. 6. Dashed lines show the same $M(T)/\mu_0 H$ curves for undoped samples ($x = 0$), scaled on the $\mathbf{y}$-axis by a factor of $1 - 2x = 0.8$.

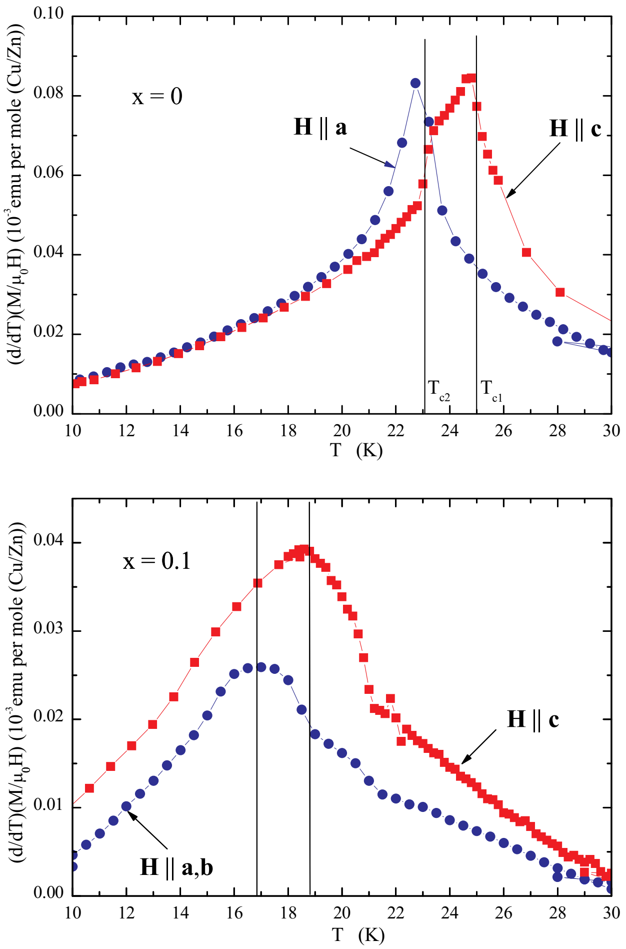

FIG. 4: (color online) Temperature dependencies of the magnetization derivative dM/dT for field directions $\mathbf{H} \parallel \mathbf{a}$, $\mathbf{b}$ (circles) and $\mathbf{c}$ (squares) and $\mu_0 H = 0.1$ T for twinned doped single crystals of $\mathrm{Li(Cu}_{1-x}\mathrm{Zn}_x)_2\mathrm{O}_2$ with $x = 0.1$ (lower panel) and for the undoped untwinned crystal $x = 0$ (upper panel, taken from Ref. 6). Data are obtained from $M(T)/\mu_0 H$ at $\mu_0 H$ =0.1 T.

our single-crystalline samples obtained with this method coincide with the values x_0 of the zinc concentration in the initial charge with precision better than $x_0 \pm 0.03$ for all samples with $x < x_c$.

The dependence of the crystal cell parameters a,b,c of the single crystals of $\mathrm{Li(Cu}_{1-x}\mathrm{Zn}_x)_2\mathrm{O}_2$ on zinc concentration x in initial charge is shown in Fig. 2. The solid symbols show the results obtained from the samples described above. In contrast with the data of Ref. 7 (open symbols), we did not observe any anomaly in the concentration dependence of the cell constants at $x = 0.055$.

Magnetization curves in static magnetic fields of up to 7 T were measured with a commercial SQUID magnetometer (Quantum Design MPMS-XL7).

The ESR experiments were performed with a transmission–type spectrometer using resonators in the frequency range $18 < \nu < 120$ GHz. The magnetic field of a superconducting solenoid was varied in the range of $0 < \mu_0 H < 8$ T. Temperatures were varied within the range of $1.2 < T < 30$ K.

The NMR experiments were performed with a conventional phase coherent, homemade pulse spectrometer at a fixed frequency of $\nu = 61$ MHz. We investigated the ^{7}Li ($I = 3/2$, $\gamma/2\pi = 16.5466$ MHz/T) nuclei using spin–echo technique with a pulse sequence 5μs–τ_D–10μs, where the time between pulses, τ_D, was 40 μs. The spectra were collected by sweeping the applied magnetic field between $3.5 < \mu_0 H < 3.9$ T. The temperatures were stabilized with a precision better than 0.02 K.

IV. EXPERIMENTAL RESULTS

A. Magnetization measurements

The experimental curves $M(T)/\mu_0 H$ and their temperature derivatives for different field directions $\mathbf{H} \parallel \mathbf{a}, \mathbf{b}$ and $\mathbf{H} \parallel \mathbf{c}$ at $\mu_0 H = 0.1$ T are shown in Figs. 3 and 4. The dependencies were obtained on the single crystal without doping ($x = 0$) and on the twinned single crystal with $x = 0.1$. For all field directions broad maxima of $M(T)/\mu_0 H$ were observed at $T = 38$ K for samples without doping and at $T = 31$ K for doped samples with $x = 0.1$. The maximum is typical for low-dimensional antiferromagnets. In the paramagnetic region, the magnetic susceptibility for $\mathbf{H} \parallel \mathbf{c}$ exceeds that for $\mathbf{H} \parallel \mathbf{a}, \mathbf{b}$, which is consistent with the anisotropy of the g-tensor measured in the ESR experiments[17] ($g_{a,b} = 2.0$; $g_c = 2.2$). At high temepatures $T \gtrsim 150$ K the susceptibility of the doped sample is $(20 \pm 1.2)\%$ less then that of the pure sample. This reduction is close to the factor $(1 - 2x)$ expected if all Zn^{2+} ions take the places of the Cu^{2+} ions, which would result in the corresponding decrease of the number of paramagnetic spins. To emphasize this fact the $M(T)/\mu_0 H$ dependency for the sample without doping reduced by factor 0.8 is shown in the same figure with dashed lines. This experiment allows to conclude that the number of magnetic Cu^{2+} ions in the doped samples of $\mathrm{Li(Cu_{1-x}Zn_x)_2O_2}$ is reduced by the number of nonmagnetic Zn^{2+} ions.

The transitions to the magnetically ordered states at T_{c1} and T_{c2} are marked by the change of the $M(T)/\mu_0 H$ slope. These inflection points are well resolved in the temperature derivative of $M(T)/\mu_0 H$ for the undoped sample (Fig. 4). The $(d/dT)(M(T)/\mu_0 H)$ curves are strongly anisotropic[6]: for $\mathbf{H} \parallel \mathbf{b}$ and $\mathbf{c}$, there are two anomalies corresponding to two transitions at T_{c1} and T_{c2}. The temperature dependence of $(d/dT)(M(T)/\mu_0 H)$ for $\mathbf{H} \parallel \mathbf{a}$ shows only one sharp peak at the lower temperature near T_{c2} in the studied field range. For the doped sample the inflection points on the $M(T)/\mu_0 H$ curves were smoothed, but the maximum of the slope for $\mathbf{H} \parallel \mathbf{c}$ was observed at evidently higher temperature than for $\mathbf{H} \parallel \mathbf{a}, \mathbf{b}$. The distance between the maxima for doped samples with $x < 0.1$ are almost the same as for the samples without doping (Fig. 4). Thus the double-step transition in the magnetically ordered phase also takes place for doped samples. Note here that the double-stage transition is specific for a planar spin structure with a strong easy-plane anisotropy for the vector $\mathbf{n}$ normal to the spin plane. The anomaly of $M(H)$ at a field of $\mu_0 H_{c1} \approx 2$ T for $\mathbf{H} \parallel \mathbf{b}$ which was associated with the reorientation of the spin plane observed earlier for samples without doping[6] was not observed for all studied samples with $x \geq 0.025$.

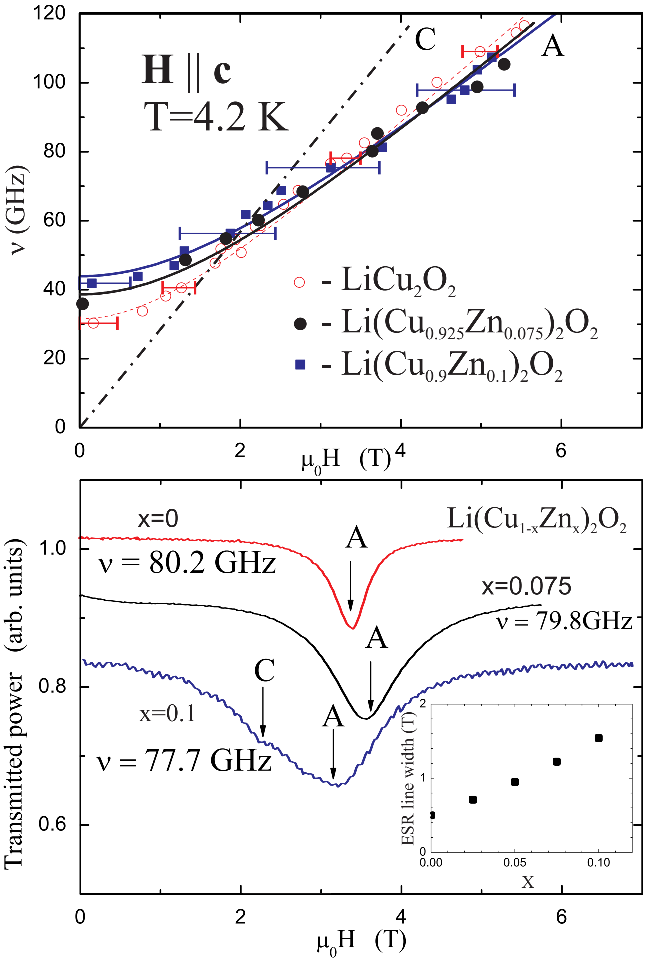

FIG. 5: (color online) Upper panel: ESR frequency-field dependency for $\mathrm{Li(Cu_{1-x}Zn_x)_2O_2}$ samples with $x = 0.075$, $x = 0.1$ (black and blue solid symbols), and $x = 0$ (open symbols, from Ref.14), $\mathbf{H} \parallel \mathbf{c}$, $T = 4.2$ K. Solid and dashed lines show fitting of the spectra with the equation given in the text. The dash-dotted line shows the spectra of the absorption component "C", which coincides with the EPR spectra measured at $T > T_N$. Lower panel: Example of ESR absorption spectra measured on three samples with $x = 0.1$, $x = 0.075$, and $x = 0$ at close frequencies ($\nu \approx 79$ GHz), $\mathbf{H} \parallel \mathbf{c}$ and $T = 4.2$ K. Insert to the lower panel: dependence of the "A"-component ESR line width on the Zn concentration. $\mathbf{H} \parallel \mathbf{c}$, $T = 4.2$ K, $\nu \approx 79$ GHz.

B. Electron Spin Resonance experiments

The ESR in single crystals of $\mathrm{Li(Cu_{1-x}Zn_x)_2O_2}$ was studied on the samples with $x = 0.025, 0.05, 0.075, 0.1$. The samples with $x = 0.025$ and $x = 0.1$ were untwinned. ESR on the sample without doping was studied in a previous work.[14] The typical ESR absorption lines are shown in the lower panels of Figs. 5 and 6. We present the lines for the samples with the Zn concentration $x = 0.075$, $x = 0.1$ and the undoped untwinned sample from Ref. 14. The ESR absorption lines are systematically broader for the samples with larger Zn concentration. The insert in

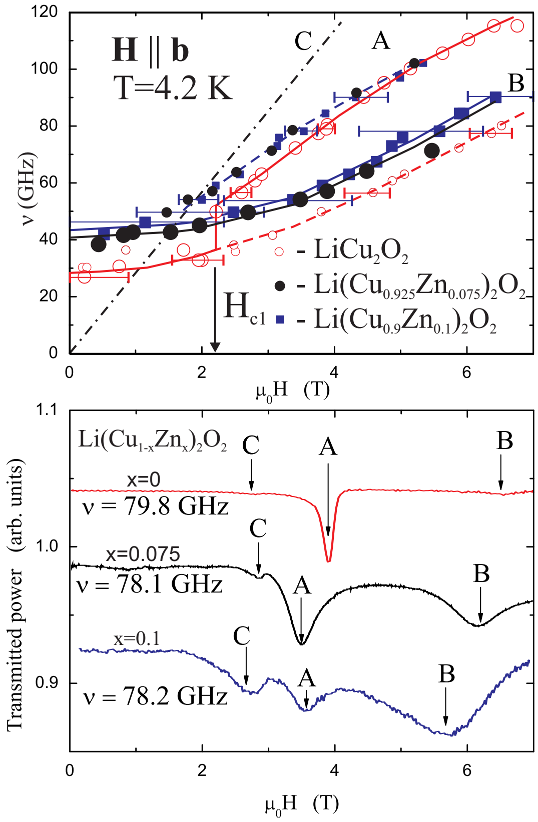

FIG. 6: (color online) Upper panel: ESR frequency-field dependencies for $Li(Cu_{1-x}Zn_x)_2O_2$ samples with $x = 0.075$, $x = 0.1$ (black and blue solid symbols), and $x = 0$ (open symbols, from Ref.14). Intense components are marked by large symbols, weak components are marked by small symbols, respectively, for $\mathbf{H} \parallel \mathbf{b}$, $T = 4.2$ K. The solid and dashed lines are guides to the eyes. The dash-dotted line corresponds to the absorption component "C", which coincides with the EPR spectra measured at $T > T_N$. Lower panel: Example of field dependencies of the transmitted power, measured on three samples with $x = 0.1$, $x = 0.075$, and $x = 0$ at two close frequencies ($\nu \approx 79$ GHz), $\mathbf{H} \parallel \mathbf{b}$ and $T = 4.2$ K.

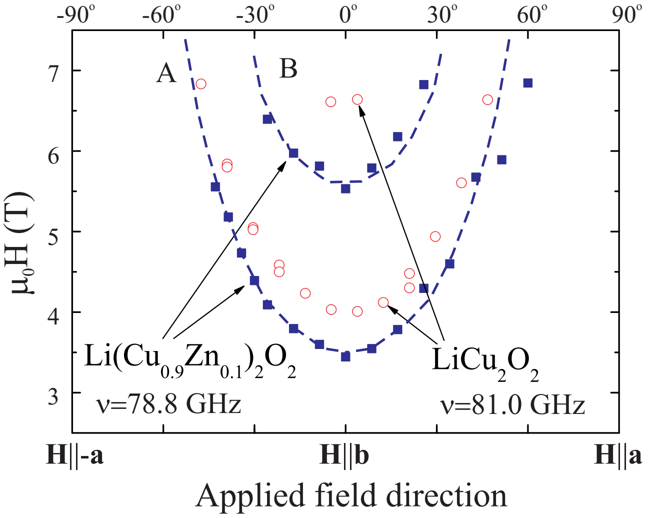

FIG. 7: (color online) (ab)-plane angular dependencies of the resonance fields for "A" and "B" components measured on $Li(Cu_{1-x}Zn_x)_2O_2$ samples with $x = 0.1$ (solid symbols), and $x = 0$ (open symbols) for frequencies around 80 GHz. $T = 4.2$ K. The dashed lines are guides to the eyes.

the lower panel of Fig. 5 shows the concentration dependence of the absorption line width for $\mathbf{H} \parallel \mathbf{c}$ at $T = 4.2$ K. The ESR spectra $\nu(H)$ for field directions $\mathbf{H} \parallel \mathbf{c}, \mathbf{b}$ for the samples with $x = 0, 0.075$ and 0.1 are shown in the upper panels of Fig. 5 and 6. The sample with $x = 0.05, 0.075$ were twinned, but due to strong anisotropy (see below) it was simple separate the absorption lines only from the domain with $\mathbf{H} \parallel \mathbf{b}$. The dash-dotted lines in the upper panels of Fig. 5 and 6 depict spectra of electron paramagnetic resonance for $LiCu_2O_2$: $\nu = (g\mu_B/h)H$ ($g_{a,b} = 2.0$; $g_c = 2.2$).[17] Resonance fields of the relatively weak component "C" are well described by such a paramagnetic dependence. Probably, this component is due to paramagnetic inclusions.

The experimental data which correspond to the absorption component "C" are not shown in the upper panels of Fig. 5 and 6. The ESR spectra $(\nu(H))$ of the intermediate Zn concentrations $x = 0.025$, $x = 0.05$ (not shown) and $x = 0.075$ interpolate between those of the samples with extreme doping concentration $x = 0$ and $x = 0.1$. The error bars on the Figs.5,6 show the antiferromagnetic resonance line widths measured at the half of the absorbed intensities.

The main features of the ESR spectra $(\nu(H))$ for different Zn concentrations remain the same as for the undoped sample. The ESR spectra $(\nu(H))$ consist of a single branch for $\mathbf{H} \parallel \mathbf{c}$ and two branches for $\mathbf{H} \parallel \mathbf{b}$. The gap of the spectra $\nu(H)$ grows from $\nu(H = 0) = 30 \pm 2$ GHz for the undoped sample ($x = 0$) to $\nu(H = 0) = 42 \pm 2$ GHz for doped samples with $x = 0.1$. Rotation of the static field into the $\mathbf{a}$-direction flattens the $\nu(H)$ dependence, which finally becomes field independent for $\mathbf{H} \parallel \mathbf{a}$.[14] Angular dependencies of the resonance fields on rotation in the (ab)-plane for samples with $x = 0, 0.1$ are shown in Fig. 7. Both resonance fields shift to higher fields as $\mathbf{H}$ approaches $\mathbf{H} \parallel \mathbf{a}$. Such a behavior was observed also for a rotation of the applied magnetic field H into the (ac)-plane. From these data we conclude that the strong uniaxial anisotropy along the $\mathbf{a}$-direction remains for all studied doped samples. Such an anisotropy corresponds to the easy (bc)-plane anisotropy for the vector $\mathbf{n}$ normal to the spin plane.

The branches marked as "A" for $\mathbf{H} \parallel \mathbf{b}, \mathbf{c}$ are quasi linear with field: $\nu = k\sqrt{H^2 + \Delta^2}$. The coefficient k is noticeably smaller than the gyromagnetic ratio $g\mu_B/h$. Such a field dependence is typical for a planar spin structure with strong "easy-plane" anisotropy for vector $\mathbf{n}$ perpendicular to the spin plane and field direction perpendicular to the anisotropy axis ($\mathbf{H} \perp \mathbf{a}$).[14] The coefficient k is defined by the anisotropy of the susceptibility of the spin structure: $k = (g\mu_B/h)\sqrt{(\chi_\parallel/\chi_\perp - 1)}$ (here $\chi_\parallel$ and

$\chi_\perp$ are the susceptibilities for field directions parallel and perpendicular to the vector **n** of the spiral spin structure). Using the value of k as a fit parameter we obtained that the anisotropy of the susceptibility $\chi_\parallel/\chi_\perp - 1$ slightly decreases from 0.55 ± 0.02 to 0.5 ± 0.02 with the increase of doping from $x = 0$ to $x = 0.1$.

For the field orientation $\mathbf{H} \parallel \mathbf{b}$ the magnetic structure of the undoped $LiCu_2O_2$ samples undergoes a reorientation at a field of $\mu_0 H_{c1} \approx 2$ T. Earlier experiments have shown that at this field the spin plane of the spiral structure rotates from the (ab) to the (ac)-plane.[6,14] The magnetic susceptibility at this field undergoes a step like increase. The ESR frequency-field dependence for this orientation is shown in the upper panel of Fig. 6. The transition field H_{c1} is marked by the jump of the frequency-field dependence for the undoped sample. The intensive component of the ESR absorption line changes form the “B”-branch of the frequency-field diagram to the “A”-branch at the transition field H_{c1} for the undoped sample. Thus, the “A”-component dominates the absorption spectrum of the undoped sample at high fields (Figure 6). For the doped sample with $x = 0.1$ the absorption component “B” was more than 10 times more intensive than the component “A” in the whole field range. No jumps of the position of the intense component in the frequency-field diagram was observed for the doped samples.

From these observations we conclude that for doped samples no magnetic reorientation takes place in the studied field range. This conclusion is in agreement with the absence of anomalies in the $M(H)$ curves mentioned in the previous subsection. Note that the value of H_{c1} and the sharpness of the transition are strongly dependent on the quality of the samples even for the crystals without doping.[6,14]

C. Nuclear Magnetic Resonance experiments

The magnetic structure of the single crystals of $Li(Cu_{1-x}Zn_x)_2O_2$ with $x = 0.1$ was tested with the NMR technique. ^{7}Li NMR field-sweep spectra measured at different temperatures at field orientation $\mathbf{H} \parallel \mathbf{c}$ and fixed frequency $\nu = 61.0$ MHz are shown in Fig. 8. The shape of the NMR spectra transforms from a single component spectrum at high temperatures $T > T_N$ to a spectrum with characteristic shoulders at temperatures below $T_N \approx 18$ K (see Fig. 8). The spin echo NMR signal in the low temperature range was observed in a broad field range $\mu_0 \Delta H \approx 0.25$ T which is approximately the same as for $LiCu_2O_2$ without doping (see Fig. 9). At temperatures close to T_N the central line of the NMR spectra dominates. This fact demonstrates, that by nearing to Neel temperature the number of nuclei with paramagnetic environment increases.

In Fig. 9 the lines show the fitting results of the NMR spectra. The ^{7}Li NMR spectra for doped and undoped samples were fitted by taking into account dipolar fields within the model of a planar spiral magnetic structure in the (ab)-plane with an incommensurate wave vector $k_{ic} = 0.827 \times 2\pi/b$ aligned along the **b**-direction and an effective magnetic moment on the Cu^{2+} position equal to $0.8\mu_B$. Note, that the contribution of the contact field for such spin arrangement $(\mathbf{H} \parallel \mathbf{c})$ can be neglected. The magnetic structure for the sample without doping is described by Eqn.(1). The mutual orientation of the spins from neighboring (ab)-planes defined by phases $\phi_{\alpha,\beta,\gamma,\delta}$ are given in the end of the section II. The line width of individual groups of resonating lithium nuclei for this computation was taken as $\delta H = 0.005$ T, which is much smaller than all peculiarities on the experimental spectra. This value of δH roughly corresponds to the value of quadrupolar splitting of NMR line on ^{7}Li nuclei in $LiCu_2O_2$ ($\nu_q \approx 51.7$ kHz, Ref. 5).

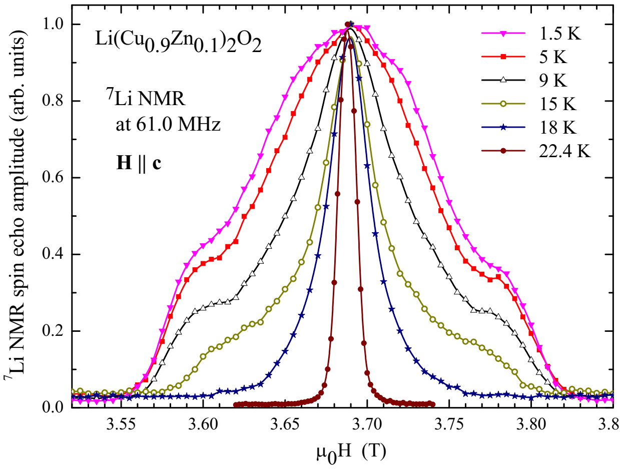

FIG. 8: (color online) NMR spectra of ^{7}Li nuclei in $Li(Cu_{1-x}Zn_x)_2O_2$, $x = 0.1$, measured at different temperatures. $\mathbf{H} \parallel \mathbf{c}$ and pumping frequency $\nu = 61.0$ MHz.

To explain the main features of our experimentally observed NMR spectra we consider effective fields at lithium sites which are generated by an individual magnetic chain of Cu^{2+} ions nearest to the lithium nuclei (see the fragment of the spiral structure shown in Fig. 1c). For simplicity we suppose that the Li^+ ion, the Cu^{2+} chain, the spin vectors, and the applied static field **H** lies in the plane of the figure. The projection of the effective field from neighboring spins on the applied field **H** changes along the spin chain sinusoidally. For a given propagation vector k_{ic} the NMR spectra exhibit a shape with two characteristic maxima at the extremum fields $\nu/\gamma \pm H_{extr}$. Since the Li^+ ions are located symmetrically between two Cu^{2+} ions, the extreme fields H_{extr} will correspond to the arrangement of the spins in the copper chain symmetric with respect to the chosen Li ion (marked with index i in Fig. 1c). As it is schematically shown in Fig. 1c, such a symmetric arrangement corresponding to the magnetic structures, with opposite wave vectors k_{ic} (solid arrows) and $-k_{ic}$ (dotted arrows), yields different dipolar contributions to effective field. Thus for

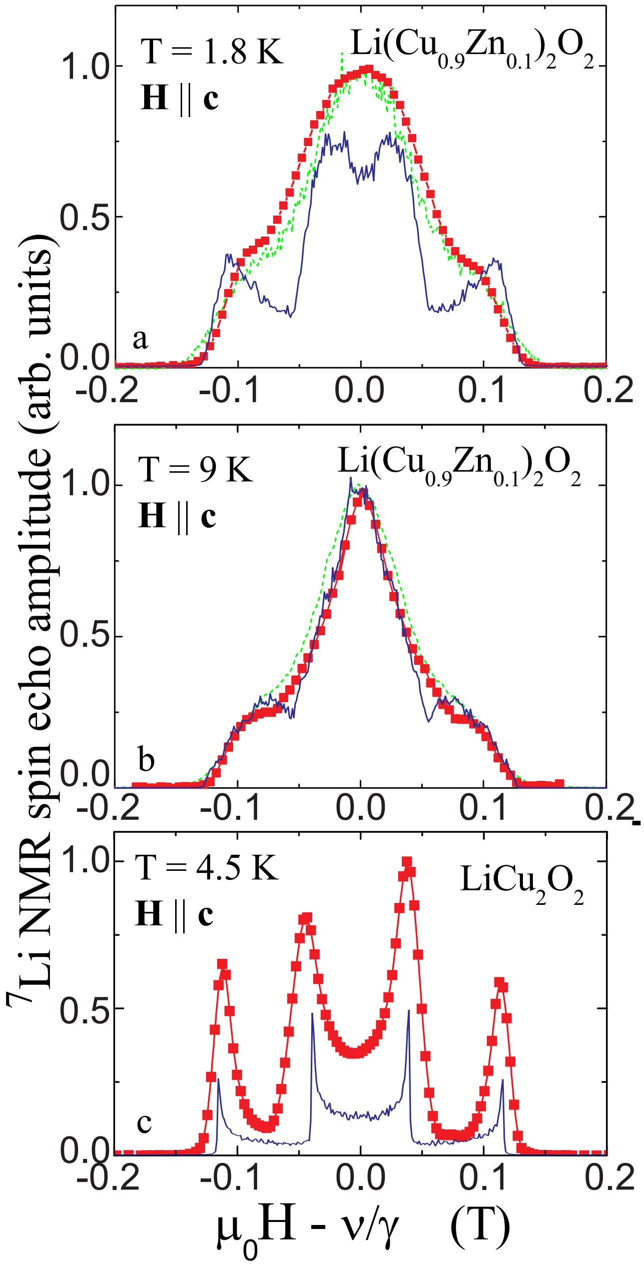

FIG. 9: (color online) Squares represent NMR spectra of ^{7}Li nuclei in $Li(Cu_{1-x}Zn_x)_2O_2$, $x = 0.1$ (top and middle panels) and $x = 0$ (bottom panel) measured at $T < T_N$ for $\mathbf{H} \parallel \mathbf{c}$ and $\nu = 61.0$ MHz. The solid lines show the simulated spectra in models of spiral planar spin structures within the (ab)-plane with long-range order in the **c**-direction for the undoped sample (bottom panel) and with disorder in the **c**-direction for the doped sample (top and middle panel). The dashed lines show the simulated spectra in the models of randomly disturbed planar spiral spin structure within *ab*-planes with short-range order in *c*-direction (top and middle panels).

such simple model structure we can expect a broad NMR spectrum with four characteristic maxima corresponding to two magnetic domains with opposite wave vectors.

The magnetic structure expected for LiCu2O2 at an arbitrary orientation of the applied magnetic field provides NMR spectra with 8 maxima corresponding to the four extremal fields at the lithium nuclei from different positions Li1, Li2, Li3, and Li4 (Fig 1b). For the field orientation $\mathbf{H} \parallel \mathbf{c}$ the number of maxima of the spectra is reduced to four (see bottom panel of Fig. 9).

In order to interpret the NMR spectra of doped samples we simulated the NMR spectra for the structures with random static deviations of the spin directions from the spin orientations of undoped model. For modeling purposes the deviation angles within the spin plane were set to the random value $-\phi^{(max)} < \phi < \phi^{(max)}$, where the maximal deviation ϕ_{max} was used as a model fitting parameter. Taking into account that the exchange interactions between planes is weaker than the in-plane interactions, we used different deviation parameters $\phi_{\parallel}^{(max)}$ for spins within (ab)-plane, and $\phi_{\perp}^{(max)}$ for spins from different planes. The NMR spectra of doped samples at 9 K can be fitted in the model of totally random mutual orientation of the spins of the neighbor planes, i.e. $\phi_{\perp}^{(max)} = 180°$ (see bottom panel of Fig.9). The NMR spectra obtained in this model are only weakly sensitive to the disorder within the individual spin plane. The solid blue line shows the computed NMR spectra with the assumption of ordered moments within each (ab)-plane ($\phi_{\parallel}^{(max)} = 0°$). The doted green line shows NMR spectra obtained under the assumption that the spin directions of ions within the (ab)-planes are oriented randomly around undisturbed directions within the angle $\phi_{\parallel}^{(max)} = 35°$. For the fit we took $0.8\mu_B$ as the absolute value of the magnetic Cu^{2+} moments at this particular temperature of $T = 9$ K. Decreasing the temperature the central maximum of the spectra start to broaden (see Fig. 8). Such transformation can be explained by the appearance of increasing spin correlations between ions of neighboring (ab)-planes towards lowering the temperature. The NMR spectrum measured at 1.8 K (squares) and the fitting results (lines) are given in the top panel of Fig. 9. Again, the solid blue line shows the computed NMR spectrum with the assumption of ordered moments within each (ab)-plane ($\phi_{\parallel}^{(max)} = 0°$) and random deviations of nearest spins from neighboring planes within the angle $\phi_{\perp}^{(max)} = 45°$. A better agreement between our model and the low-temperature experimental NMR spectrum is obtained for the case of a magnetic structure with short ranged static correlations for both in-plane and inter-plane correlations according to the green dashed line. It shows the computed NMR spectrum with the assumption of random deviations of spins described by the parameters $\phi_{\parallel}^{(max)} = \phi_{\perp}^{(max)} = 35°$. Again, the absolute value of the magnetic moments of Cu^{2+} was taken to be $0.8\mu_B$ for the fit. Here we must note that the local field at the probing nuclei is defined mostly by four nearest coordination spheres, which means that the NMR spectra are sensitive to short-range correlations only. These correlations must be static at least during the time window of ≈ 0.1 s set by our NMR experiment.

V. DISCUSSION

X-ray diffraction and electron probe micro analysis of the single-phase crystals of $\mathrm{Li(Cu_{1-x}Zn_x)_2O_2}$ show that Zn ions enter into the lattice without destruction of the crystal structure in the broad concentration range $0 \leq x \lesssim 0.12$. The scaling of the high-temperature susceptibility as $(1-2x)$, shown in the Figure 3, indicates that Zn ions substitute for $\mathrm{Cu^{2+}}$ and each $\mathrm{Zn^{2+}}$ ion reduces the number of magnetic ions by one. Nonmagnetic dilution should also affect the effective interspin interactions (i.e. Weiss temperature Θ). The fit of our $H||c$ susceptibility data in the $150K-300K$ temperature range shows that the Weiss temperature decreases from $(61\pm3)K$ for the pure compound to $(51\pm5)K$ for the 10% doped compound. The Weiss temperature of the doped system is also about 80% of that for the pure compound, which is again close to the $(1-2x)$ factor describing the decrease of the average number of neighbors of the magnetic ion with doping. On the other hand, even for the 10% doping the $M(T)$ curves demonstrate the same characteristic broad maximum around $35K$ as for the pure compound. Thus, magnetization measurements prove that the magnetic subsystem of $\mathrm{Li(Cu_{1-x}Zn_x)_2O_2}$ can still be considered as a system of spins $(S=1/2)$ with frustrated exchange interactions, where the spins are arranged in chains along the crystallographic b-axis.

According to Ref. 9 the strongest exchange interactions for undoped $\mathrm{Li(Cu_{1-x}Zn_x)_2O_2}$ are the interactions between copper ions within the (ab)-planes: intrachain interactions of nearest spins J_1, intrachain interactions of next-nearest spins J_2 and interchain interaction J_3 (see Fig.1). These interactions lead to a spiral long-range magnetic order with an incommensurate wave vector directed along the crystallographic **b**-axis. The solitary nonmagnetic $\mathrm{Zn^{2+}}$ defects disturb this spiral magnetic structure in their immediate surroundings only.

For small concentrations x the characteristic size of the disturbed area around nonmagnetic defects can be evaluated as $\frac{2(J_1,J_2)}{J_3}$ cell units, which yields a value of 4 cell units in the case of $\mathrm{LiCu_2O_2}$. For $x=0.1$ the average distance between such nonmagnetic defects within the chains amounts to ≈ 5 lattice constants and, therefore, any long-range order of the magnetic structure is most likely destroyed for such highly doped compound.

We suggest that such a disordered state can be a realization of a novel spin-glass like state with short-range chiral correlations in the (ab)-planes. It is important that for the system with frustration of exchange interactions discussed here, the replacement of magnetic ions by nonmagnetic does not break the exchange bond within the chains, because such replacement excludes nearest but not next-nearest bonds. This circumstance can be the reason of the relatively weak reduction of the ordering temperature by doping of the samples observed experimentally.

The ESR experiments show that the main features of the low-frequency spectrum of excitations in $\mathrm{Li(Cu_{1-x}Zn_x)_2O_2}$ do not change at a doping of $x \leq 0.1$. The spectra can be explained in the frame of a planar spin structure with strong easy-axis anisotropy along the a-axis of the crystal. This means that the spins of this spin-glass like structure lie in the plane defined by the applied magnetic field $\mathbf{H}$ and the axial-anisotropy vector along the a-axis for all concentrations x within the entire range $0 \leq x < 0.1$. The absorption line width of $\mathrm{Li(Cu_{1-x}Zn_x)_2O_2}$ strongly increases with the Zn concentration (insert in Fig. 4) and the absorption lines of the highly doped samples are asymmetric: the low-field part of the absorption lines is more broadened than the high-field part. Probably, this asymmetry is due to a nonuniformity of the magnetic structure of the doped $\mathrm{Li(Cu_{1-x}Zn_x)_2O_2}$. The defects in the magnetic structure might trigger excitations of magnons with nonzero wave vectors (see for example Ref. 18). The resonance condition for such excitations is expected for applied magnetic fields lower than the antiferromagnetic resonance field.

The NMR experiments indicate that the value of the magnetic moments at the position of $\mathrm{Cu^{2+}}$ ions at low temperature in doped samples is nearly the same as in the samples without doping at temperatures less then 15 K. Additionally, the shape of the NMR spectra of zinc doped samples indicates short-range static correlations the same as in undoped samples. These correlations appear at the temperature ≈ 18 K, where was observed the anomaly on magnetization curve and the ESR spectra start to be gaped. The temperature evolution of the shape of NMR spectra of doped samples can be explained by appearance of short-range correlations between spins of neighbor (ab)-planes with decrease of the temperature from 9 to 1.8 K. The interpretation of the experimental spectra and our fitting results is natural and one of the simplest. But we can not exclude other models, which can describe the NMR spectra in another way. The results of NMR experiments on strongly doped $\mathrm{Li(Cu_{1-x}Zn_x)_2O_2}$, for $x=0.1$ are in agreement with the spin-glass like magnetic structure suggested above.

VI. CONCLUSIONS

Untwinned single-crystalline samples of $\mathrm{Li(Cu_{1-x}Zn_x)_2O_2}$ were grown for $0 \leq x < 0.12$. It is shown that the zinc doping diminishes the number of magnetic copper ions $\mathrm{Cu^{2+}}$ and a single crystallographic phase is maintained for all samples within the entire doping range $0 \leq x < 0.12$. The ESR spectra for all doping concentrations within $0 \leq x < 0.12$ can be well explained in the model of a planar spin structure with strong easy-plane type anisotropy for the vector $\mathbf{n}$ normal to the spin plane. The NMR spectra of the highly doped single crystal $\mathrm{Li(Cu_{0.9}Zn_{0.1})_2O_2}$ can be well described by planar spin-glass like magnetic structure with static short-range spiral correlations. The value of magnetic moments of Cu^{2+} ions in this structure is close to the value obtained for undoped crystals: $(0.8 \pm 0.1)\ \mu_B$.

VII. ATTACHMENT

According to the theory of exchange symmetry[19] the order parameter in a coplanar exchange structure is represented by two mutually perpendicular unit spin vectors $\mathbf{l_1}$ and $\mathbf{l_2}$, which transform according to a particular irreducible representation of the crystal symmetry group. In a helical magnetic structure, the order parameter with respect to the subgroup of translations transforms according to the representation with an incommensurate wave vector. Lagrange function for this system can be written as

$$L = \frac{I_1}{2}((\dot{\mathbf{l}}_\mathbf{1}+\gamma[\mathbf{l_1H}])^2+(\dot{\mathbf{l}}_\mathbf{2}+\gamma[\mathbf{l_2H}])^2)+\frac{I_2}{2}(\dot{\mathbf{n}}+\gamma[\mathbf{nH}])^2-U_a,$$

where $\mathbf{n} = [\mathbf{l_1 l_2}]$, and U_a - small addition to the exchange part of the energy due to relativistic effects. $\mathbf{I_i}$ and the susceptibility tensor components are related by the expressions: $\chi_\perp = I_1 + I_2, \chi_\parallel = 2I_1$. In the spiral magnetic structure, U_a depends only on the orientation of the vector $\mathbf{n}$ with respect to the crystal axes. In the simplest case, when the direction of all the spirals coincide, senior terms in the expansion of the quantity U_a in the components of the vector n for a biaxial crystal can be written as $\frac{1}{2}(An_z^2 + Bn_y^2)$. For a magnetic field directed along one of the symmetry axes, vector $\mathbf{n}$ also directed along one of the twofold axes. The coordinate axes are chosen so that, in a zero magnetic field, the vector $\mathbf{n}$ is parallel to the $\mathbf{z}$-axis. Then, the coefficients A and B satisfy the inequalities $A < 0,\ A < B$. In the absence of the magnetic field, oscillation frequencies are

$$\omega_{10}^2 = \frac{-A}{\chi_\perp},\ \omega_{20}^2 = \frac{B-A}{\chi_\perp},\ \omega_{30} = 0$$

The third oscillation frequency is equal to zero also for $H \neq 0$. In the magnetic field directed along the $\mathbf{z}$-axis, the resonance frequencies are determined by the formula

$$\omega_{1,2}^2 = \frac{\omega_{10}^2+\omega_{20}^2}{2} + \gamma^2H^2\frac{I_1^2+I_2^2}{(I_1+I_2)^2} \pm \pm\left(\frac{(\omega_{10}^2-\omega_{20}^2)^2}{4} + 2(\omega_{10}^2+\omega_{20}^2)\gamma^2H^2\frac{I_2^2}{(I_1+I_2)^2} + + 4\gamma^4H^4\frac{I_1^2I_2^2}{(I_1+I_2)^4}\right)^{1/2}. \quad (2)$$

For $\mathbf{H} \parallel \mathbf{y}$

$$\omega_1^2 = \omega_{10}^2,\ \omega_2^2 = \omega_{20}^2 + \gamma^2H^2$$

For $\mathbf{H} \parallel \mathbf{x}$

$$\omega_1^2 = \omega_{10}^2 + \gamma^2H^2,\ \omega_2^2 = \omega_{20}^2$$

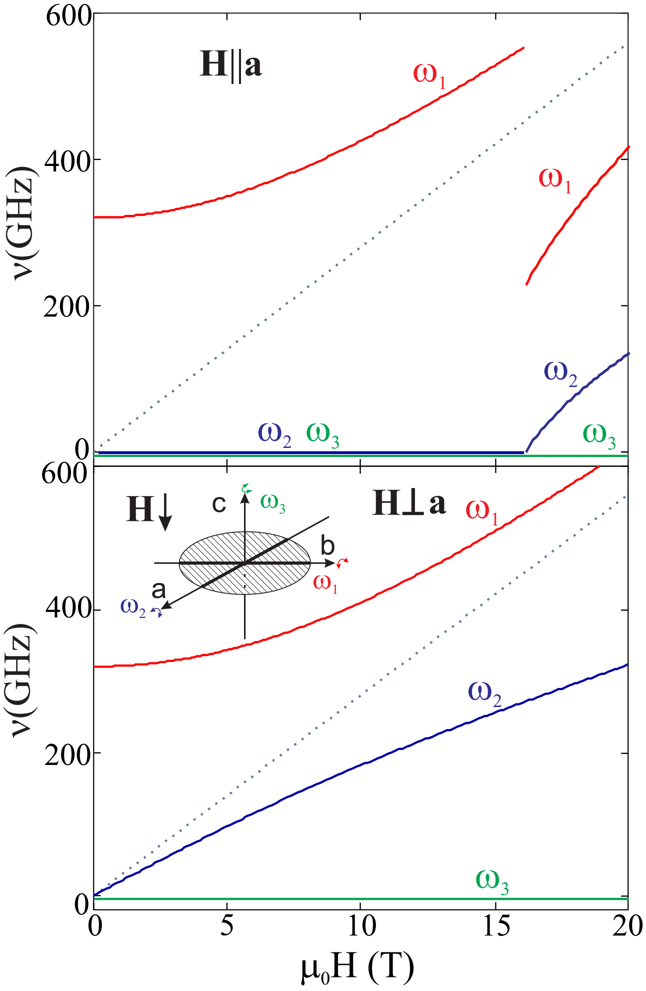

FIG. 10: (color online) The calculated ESR spectra of the planar spiral antiferromagnet with uniaxial anisotropy and parameters of $LiCu_2O_2$ (ω_{10} = 320 GHz, ω_{20} = 0 GHz and $\sqrt{\frac{\chi_\perp}{\chi_\parallel-\chi_\perp}} = 1.4$). Solid lines show the spectra. Top panel: $\mathbf{H}\|\mathbf{a}$. Bottom panel: $\mathbf{H} \perp \mathbf{a}$. Dotted line indicate the paramagnetic resonance spectra. Insert to the bottom panel: the scheme of oscillations of the spin plane at $\mathbf{H}\|\mathbf{c}$.

The reorientation transitions occurs in the following fields:

If $\chi_\perp > \chi_\parallel$ and $\mathbf{H} \parallel \mathbf{z}$

$$H_{cz} = \frac{min(\omega_{10},\omega_{20})}{\gamma}\sqrt{\frac{\chi_\perp}{\chi_\perp-\chi_\parallel}}$$

And if $\chi_\perp < \chi_\parallel$ and $\mathbf{H}$ directed along $\mathbf{x}$ or $\mathbf{y}$

$$H_{cx} = \frac{\omega_{10}}{\gamma}\sqrt{\frac{\chi_\perp}{\chi_\parallel-\chi_\perp}},\ H_{cy} = \frac{\omega_{20}}{\gamma}\sqrt{\frac{\chi_\perp}{\chi_\parallel-\chi_\perp}},$$

respectively. In the first case, the oscillation frequencies in fields above the field of the spin-flop are given by

$$\omega_1^2 = \frac{A}{\chi_\perp} + \gamma^2H^2,\ \omega_2^2 = \frac{B}{\chi_\perp},$$

$$\omega_1^2 = \frac{-B}{\chi_\perp} + \gamma^2 H^2,\ \omega_2^2 = \frac{A-B}{\chi_\perp},$$

depending on whether the constant B is positive ($\mathbf{n} \parallel \mathbf{x}$ at $H > H_{cz}$) or negative ($\mathbf{n} \parallel \mathbf{y}$ in $H > H_{cz}$). In the second case, the frequencies are determined by expression (1), into which is necessary to substitute

$$\omega_{10}^2 = \frac{A}{\chi_\perp},\ \omega_{20}^2 = \frac{B}{\chi_\perp}$$

for $\mathbf{H} \parallel \mathbf{x},\ H > H_{cx}$ and

$$\omega_{10}^2 = \frac{-B}{\chi_\perp},\ \omega_{20}^2 = \frac{A-B}{\chi_\perp}$$

for $\mathbf{H} \parallel \mathbf{y},\ H > H_{cy}$

In a more complex case, where not all the spirals twisted to one side, in the expansion of U_a can also add member Cn_y. In this case, as well as the fields are not directed along the axes of symmetry of the crystal, expressions for the frequencies are too bulky and the orientation of the order parameter and the frequency of small oscillations are found by numerical calculations of the equilibrium orientation of the order parameter, relative to the crystal axes and the frequencies of small oscillations.

Fig. 10 shows the calculated spectra for $LiCu_2O_2$ in the model of planar spiral antiferromagnet with uniaxial anisotropy and parameters: $\omega_{10} = 320$ GHz, $\omega_{20} = 0$ GHz and $\sqrt{\frac{\chi_\perp}{\chi_\parallel - \chi_\perp}} = 1.4$.

Acknowledgments

We are thankful for the useful and enlightening discussions to S. S. Sosin. This work is supported by the Grants 12-02-00557-a, 10-02-01105-a, 11-02-92707-IND-a of the Russian Foundation for Basic Research, Program of Russian Scientific Schools, and by the German Research Society (DFG) within the Transregional Collaborative Research Center (TRR 80).

---

[*] Electronic address: svistov@kapitza.ras.ru

[1] T. Hikihara, L. Kecke, T. Momoi and A. Furusaki, Phys. Rev. B **78**, 144404 (2008).

[2] J. Sudan, A. Lüscher, and A. M. Läuchli, Phys. Rev. B **80**, 140402(R) (2009).

[3] A. F. Andreev, I. A. Grishchuk, Sov. Phys. JETP **60**, 267 (1984).

[4] T. Masuda, A. Zheludev, A. Bush, M. Markina, and A. Vasiliev, Phys. Rev. Lett. **92**, 177201 (2004).

[5] A. A. Gippius, E. N. Morozova, A. S. Moskvin, A. V. Zalessky, A. A. Bush, M. Baenitz, H. Rosner, and S.-L. Drechsler, Phys. Rev. **70**, 020406 (2004).

[6] A. A. Bush, V. N. Glazkov, M. Hagiwara, T. Kashiwagi, S. Kimura, K. Omura, L. A. Prozorova, L. E. Svistov, A. M. Vasiliev, A. Zheludev, Phys. Rev. B **85**, 054421 (2012)

[7] H. C. Hsu, J.-Y. Lin, W. L. Lee, M.-W. Chu, T. Imai, Y. J. Kao, C. D. Hu, H. L. Liu, and F. C. Chou, Phys. Rev. B **82**, 094450 (2010).

[8] R. Berger, A. Meetsma, S. v. Smaalen, J. Less-Common Met. **175**, 119 (1991)

[9] T. Masuda, A. Zheludev, B. Roessli, A. Bush, M. Markina, and A. Vasiliev, Phys. Rev. **72**, 014405 (2005).

[10] S. Seki, Y. Yamasaki, M. Soda, M. Matsuura, K. Hirota, and Y. Tokura, Phys. Rev. Lett. **100**, 127201 (2008).

[11] Y. Kobayashi, K. Sato, Y. Yasui, T. Moyoshi, M. Sato, and K. Kakurai, J. Phys. Soc. Jpn. **78**, 084721 (2009).

[12] A. Rusydi, I. Mahns, S. Müller, M. Rübhausen, S. Park, Y. J. Choi, C. L. Zhang, S.-W. Cheong, S. Smadici, P. Abbamonte, M. v. Zimmermann, and G. A. Sawatzky, Appl. Phys. Lett. **92**, 262506 (2008).

[13] S. W. Huanga, D. J. Huanga, J. Okamoto, W. B. Wu, C. T. Chen, K. W. Yeh, C. L. Chen, M. K. Wu, H. C. Hsu, F. C. Chou, Sol. State Com. **147**, 234 (2008).

[14] L. E. Svistov, L. A. Prozorova, A. M. Farutin, A. A. Gippius, K. S. Okhotnikov, A. A. Bush, K. E. Kamentsev, and É. A. Tishchenko, JETP **135**, 1151 (2009).

[15] L. E. Svistov, L. A. Prozorova, A. A. Bush, K. E. Kamentsev, J. Phys.: Conf. Series **200**, 022062 (2010)

[16] A. A. Bush, K. E. Kamentsev, E. A. Tishchenko, Inorganic Materials **40**, 44 (2004).

[17] A. M. Vorotynov, A. I. Pankrats, G. A. Petrakovski., K. A. Sablina, V. Pashkovich, and G. Shimchak, JETP **86**, 1020 (1998).

[18] H. - A. Krug von Nidda, L. E. Svistov, L. A. Prozorova, Fizika Nizkih Temperatur, **36**, 926 (2010)

[19] A. F. Andreev and V. I. Marchenko Usp. Fiz. Nauk **130**, 39, (1980).